Progress In Electromagnetics Research C, Vol. 101, 53–69, 2020

Receiving UWB Antenna for Wireless Capsule Endoscopy Communications

Chaïmaâ Kissi[1, *], Mariella Särestöniemi[2], Timo Kumpuniemi[2], Sami Myllymäki[3], Marko Sonkki[2], Juha-Pekka Mäkelä[2], Mohamed Nabil Srifi[1], Heli Jantunen[3], and Carlos Pomalaza-Raez[4]

Abstract—Wireless capsule endoscopy systems utilize a combination of hardware and software devices to ensure the healthcare of a human being. In praise of involved antennas in the overall medical system design, UWB (Ultra-Wideband) range occupies the highest ranks in the literature. The low-band of UWB is regarded as the best frequency range, within the approved standards, to realize the better transmission of captured medical images by the capsule inside the SI tract, in terms of high resolution and low-path loss. A variety of passive capsules have been designed and made available in the literature, while the accurate design of the corresponding on-body antenna is lagging. For this purpose, this paper provides an extended study of a recently published on-body antenna operating at 3.75–4.25 GHz band. The measured antenna realizes good directivity of 5.78 dBi and 9.50 dBi towards the body without and with the cavity, respectively. The direction of the proposed on-body antenna beam is targeted to be mounted on the body surface. On-body simulations were run with CST Microwave Studio by involving an abdominal multi-layer model, and followed by navel and back areas of the voxel model to predict the antenna behavior close to different lossy body environments. Later, the antenna structure was measured next to a real human abdomen. Simulation results reveal that the proposed antenna with or without the cavity enables enhanced in-body communication when mounted on the abdomen with less path loss. This is supported by the low power totaling 20 dB at the SI (Small Intestine) tract. Furthermore, on-body measurements confirm the good antenna performance. Consequently, the planar compact antenna is regarded as a good on-body candidate for wireless capsule endoscopy systems.

1. INTRODUCTION

Recently, the advancement of technologies for healthcare service has risen sharply [1–5]. The outcomes of relevant medical researches exceed laboratory attempts and are already upgraded to clinical trials [6, 7]. Medical equipment currently captures the attention of scientists increasingly. Just to name few, today, Wireless Capsule Endoscopy (WCE) is a matter of some discussions. It has made the biggest contribution in the last and current years in scientific domains, not only for troubles diagnostic [8, 9], but for biopsy [10] and drug delivery [11, 12] purposes as well. This is the field where antennas have played an essential role in one of the promoting medical research fields [13]. Despite the development of capsule device/equipment, the good operation of the on-body device is crucial. In addition to the designed capsule antenna, researchers continue to carry out valuable work to enable and sustain a good on-body to in-body communication link. On-body antennas are helpful especially when achieving good directivity

Received 22 December 2019, Accepted 3 April 2020, Scheduled 14 April 2020
* Corresponding author: Chaïmaâ Kissi (chaimaakissi1@gmail.com).
[1] Electronic Electronics and Telecommunication Systems Research Group, National School of Applied Sciences (ENSA), Ibn Tofail University, Kenitra, Morocco. [2] Centre for Wireless Communications, Faculty of Information Technology and Electrical Engineering, University of Oulu, Finland. [3] Microelectronics Research Unit, Faculty of Information Technology and Electrical Engineering, University of Oulu, Finland. [4] Department of Electrical and Computer Engineering, Purdue University, Fort Wayne, Indiana 46805, USA.

normal to the body surface. Consequently, improved wireless communication will be made possible. If enabled successfully, it is possible to derive useful information about the data transferred by the capsule. Even more, the accurate localization of the capsule can be achieved by applying efficient localization algorithm [14–16]. However, all the aforementioned issues do not complete the list of requirements. Admittedly, the frequency range is of high priority to be considered even before starting the antennas design. Regarding this issue, a set of frequency bands have been used up to date, i.e., 433 MHz ISM (Industrial, Scientific and Medical) band [17], 38.5 & 57.6 MHz dual-band [18], 0.902–0.928 GHz ISM band & 1,395–1,4 GHz WMTS (Wireless Medical Telemetry Service) bands [19], 2.4 GHz ISM band [20], MedRadio [21], etc. Nonetheless, the suitable frequency band for this specific medical application is the mandatory channel of the low UWB (Ultra-Wide Band) band, defined as 3.75–4.25 GHz pursuant to IEEE 802.15.6 standard [22, 23]. Related works, already published, argue the lack of on-body antennas designed for in-body communication with the capsule. To the authors' best knowledge, available works in literature are, most if not all, devoted only to the design of the capsule antennas working at 3.75–4.25 GHz UWB band. Explicitly, new capsule antennas are originally described in [24–27]; however, less focus and concern was given to the on-body antenna which can be seen from the standard horn and elliptical antenna structures suitable for on-body communications used in these published works. From these references, one can clearly notice that the selection of on-body antennas used in investigations did not relay on serving the targeted medical application, but are only used to establish a point-to-point communication between the internal and external antennas. In addition to the general radiation specifications of these on-body antennas, their relative large size presents a problem in practical use. Then, a compact planar antenna is advisable for the comfort of the patient in clinical use in addition to its high radiation properties/characteristics. Since the on-body antenna is meant for clinical use, the radiation safety of the exposed human body part is highly important to be tested beforehand [28, 29]. This information is not considered in the literature related to wireless capsule endoscopy topic because the papers directly provided the path loss [30] measured between the prototypes of the on-body antenna and a capsule embedded/immersed in a phantom or meat samples. In this context, this paper aims to point out the on-body issues/features of new outside antenna properly designed for wireless capsule endoscopy.

This paper is an extension of the work originally presented in [31]. To briefly summarize the original paper content, [31] introduces the proposed UWB antenna and discusses the tuning parameter impact on the antenna performances with and without cavity. The investigations were restricted to simulation-based study using two antennas to evaluate the cavity effect on the channel propagation using a multi-layer model. Hence, the previous study concluded the improvement of the channel propagation with the cavity presence. However, in this paper we extend the analysis by (1) validating the antenna performance by measurements (2) evaluating the antenna operation next to a human body by means of realistic models such as voxel models and (3) confirming these results with on-body measurement involving real human.

The paper content is organized as follows. The antenna structures of both planar/cavity approaches are briefly presented in Section 2. Section 3 describes simulation/measurement based free-space results. Simulated on-body and in-body antenna features are analyzed in Sections 4 and 5, respectively. Then, measured on-body results are discussed in Section 6. Finally, the paper is concluded by listing the open perspectives of this work.

2. ANTENNA STRUCTURE

The antenna structure proposed in this paper has been recently presented in [31]. The antenna is basically a planar structure operating at 3.75–4.25 GHz frequency band, defined in IEEE 802.15.6 standard [22, 23]. The front and back sides of the planar antenna are given in Figures 1(a) and (b), respectively in [31]. Moreover, the antenna was backed by a metallic cavity in order to improve the antenna directivity towards a human body, as illustrated in Figure 10 in [31]. The optimized parameter values of the UWB antenna with and without the cavity are resumed in Table 1 in [31].

3. FREE-SPACE ANTENNA ANALYSIS

3.1. Simulated Results

The bandwidth matching is simulated in free-space for the antenna with and without the cavity, as shown in Figure 1. In the rest of the paper the impedance bandwidth is fixed by $S_{11} < -10\,\text{dB}$. Results show that the upper frequency is fixed to 4.35 GHz regardless the cavity element. However, it appears that the lower frequency is smoothly affected by the cavity introduction. As seen from Figure 1, the lower frequency is shifted downwards from 3.7 GHz to 3.5 GHz, in the case of the cavity presence. Consequently, the antenna bandwidth is slightly widened by using the cavity to achieve 3.5–4.35 GHz. On the other hand, a fair decrease of the resonant frequency is noticed with the cavity presence from 4 GHz to 3.93 GHz. Figure 2 reveals that the antenna radiates well regardless the cavity impact. This is clearly seen from the total efficiency ranging between 0 and 1 in linear scale over the full bandwidth of interest, i.e., 3.75–4.25 GHz. The good antenna efficiency is consequent to the matching of the proposed antenna to a 50 Ω coaxial cable required in measurement process. To be explicit, the input impedances of the antenna with and without the cavity at 4 GHz are $51.93 + j6.74\,\Omega$ and $48 - j0.19\,\Omega$, respectively. Simulated 3D radiation patterns at 4 GHz of the antenna without and with the cavity are given by Figures 3(a) and (b), respectively. Details of the radiation properties are delivered in Table 1 for both antenna cases. Consequently, the maximum realized gain of the planar antenna is in Theta = 90° direction and Phi = 38° with a value of 2.4 dB. By the presence of the cavity, the gain achieves 7.4 dB in Phi = 90° direction and Theta = 17°. Spherical coordinates are described as illustrated in Figure 3.

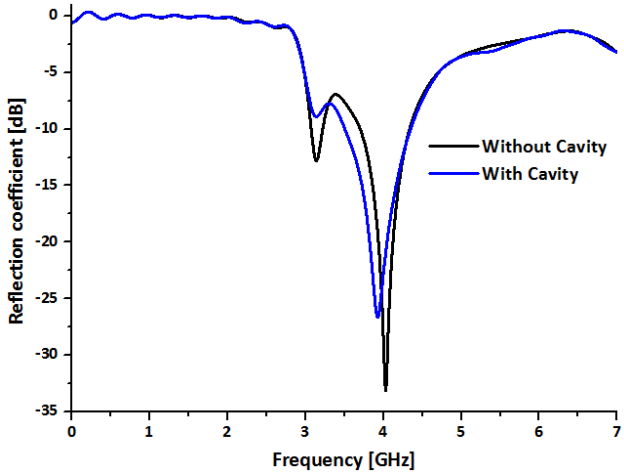

Figure 1. Simulated reflection coefficient of the UWB antenna with and without the cavity.

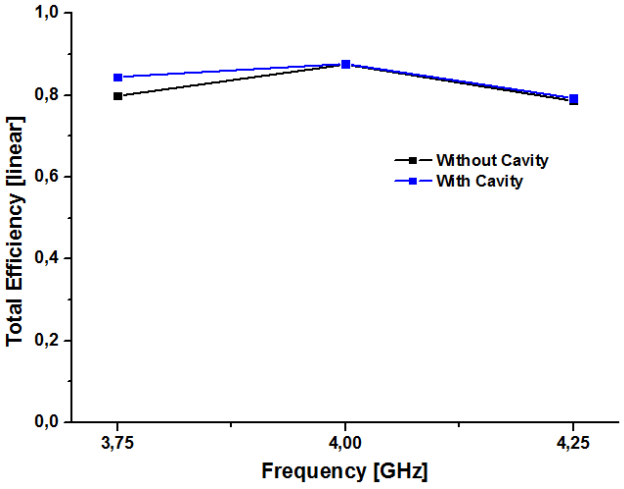

Figure 2. Simulated total efficiency of the UWB antenna with and without the cavity.

Table 1. Simulated realized gain of the proposed UWB antenna with and without the cavity.

	Without/With cavity		
Frequency [GHz]	**Phi = 0° [dB]**	**Phi = 90° [dB]**	**Theta = 90° [dB]**
3.75	0.27/5.98	1.67/6.5	2.21/−2.05
4	1.04/6.7	2.04/**7.37**	**2.39**/−1.51
4.25	1.14/6.82	1.63/7.66	1.54/−1.77

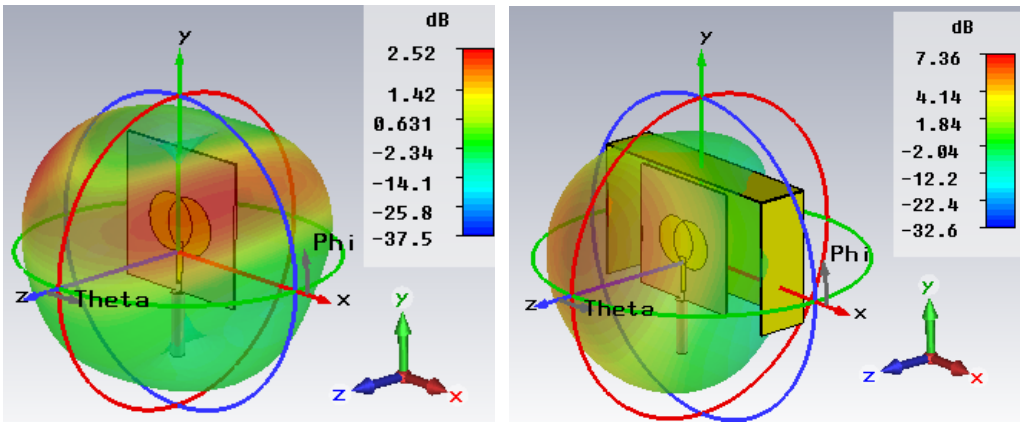

(a) (b)

Figure 3. Simulated directivity (3D overview) of the UWB antenna at 4 GHz (a) without and (b) with the cavity in free-space.

3.2. Measured Results

To validate the simulated free-space antenna performances, the antenna was fabricated, by introducing a Rohacell piece [32] properly designed to support the antenna, as pictured in Figure 4. The reflection coefficient result was measured by VNA (Vector Network Analyzer), and radiation patterns were obtained by Satimo Starlab system. In this regard, the antenna measurement system was first calibrated to UWB range by using a horn antenna depicted in Figure 5(a). Then the proposed antenna was measured, as shown in Figure 5(b), by recording results at the frequencies of interest 3.75 GHz, 4 GHz, and 4.25 GHz. According to the S-parameters presented in Figure 6, the measurement results well correlate with the simulation results reported in Figure 1. Additionally, the measured total efficiency provided in Figure 7 proves that the antenna radiates well especially at 4 GHz center frequency. Besides, the UWB antenna without cavity has an improved efficiency with the cavity at 4 GHz. The simulated and measured radiation patterns of the UWB antenna with and without the cavity at 3.75 GHz, 4 GHz, and 4.25 GHz are described in Figure 8. Details of the radiation performances of the UWB antenna with and without the cavity are compared in Table 2. Measurement results prove that the antenna with cavity achieves a maximum gain of 9.50 dB in Phi = 90° direction and Theta = 12°, at 4 GHz center frequency. Furthermore, the UWB antenna without the cavity reaches a maximum measured 5.78 dB gain in the same direction Phi = 90° with Theta = 206.8° at 4 GHz. It is clearly remarked that the increase of the measured gain of the antenna is regardless of the cavity introduction. This difference in values can be attributed to the coaxial cable effect in real measurements. Consequently, the resulting free-space measurements validate the good operation of the proposed antenna in both cases.

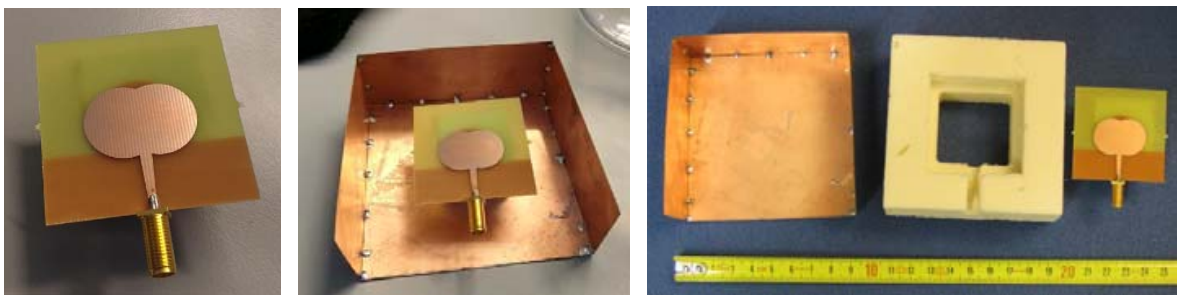

(a) (b) (c)

Figure 4. UWB antenna prototype (a) without and (b) with the cavity, (c) the three elements of the proposed antenna with cavity for on-body use.

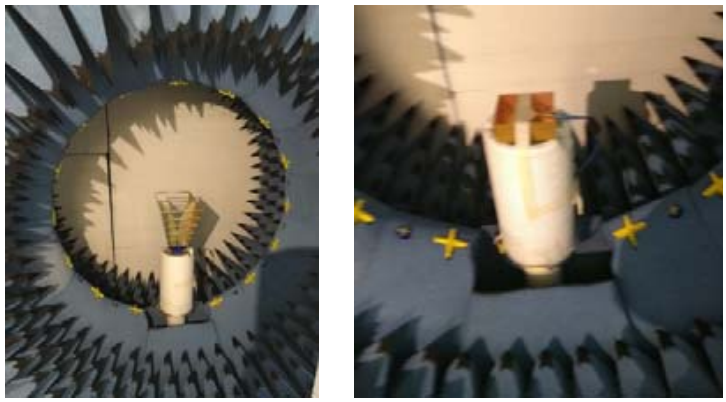

(a) (b)

Figure 5. Setup for radiation patterns measurements, in free-space, using (a) horn antenna for calibration and (b) the proposed UWB antenna with cavity.

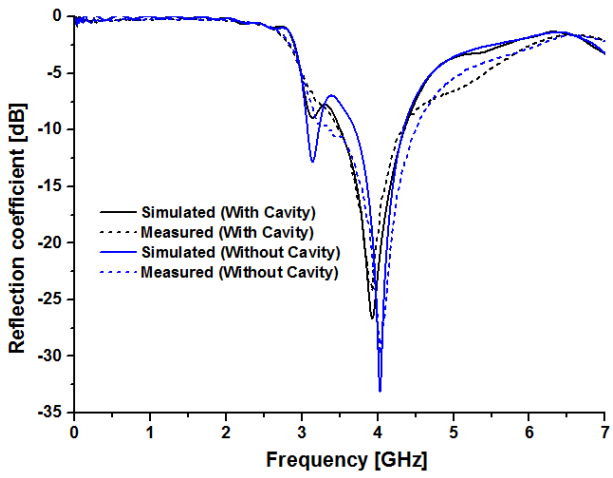

Figure 6. Simulated and measured reflection coefficient of the UWB antenna with and without cavity.

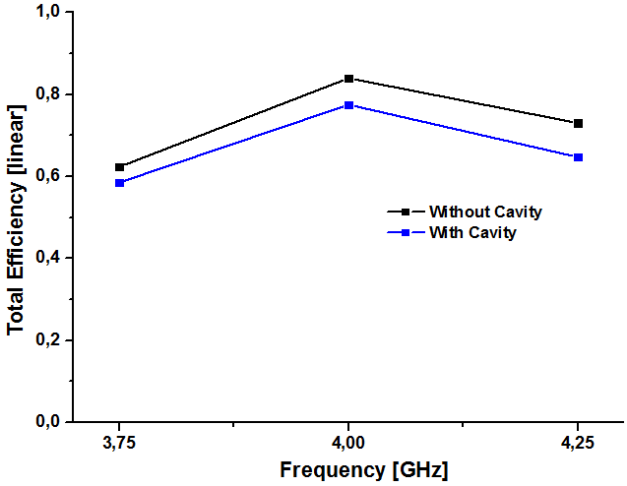

Figure 7. Measured total efficiency of the proposed UWB antenna with and without cavity.

Table 2. Measured gain of the proposed UWB antenna with and without cavity.

	Without/With cavity		
Frequency [GHz]	**Phi = 0° [dB]**	**Phi = 90° [dB]**	**Theta = 90° [dB]**
3.75	2.23/7.33	3.60/7.52	0.67/−1.90
4	3.47/9.33	**5.78/9.50**	3.36/−1.10
4.25	3.52/9.05	5.26/9.18	2.44/−0.50

4. ON-BODY ANTENNA SIMULATION ANALYSIS

The proposed antenna is designed for in-body propagation, especially the communication with an implant/capsule situated in the Small-Intestine (SI) organ. This objective leads to conduct a set of on-body simulations by emulating the body effect on the antenna properties. The body presence was emulated in CST by multi-layer and 3D voxel models, as illustrated in Figure 9 and Figure 10,

respectively. Laura voxel model 2018 from CST library is preferred because it includes all the organs needed for this specific application, called wireless capsule endoscopy. The planar layer-based model consists of the following tissues appearing in this order: Skin, Fat1, Muscle, Fat2, SI_Wall, and SI_Content placed at a fixed distance d of 4 mm, as described in Figure 9. The layered model has 150 mm-length and 110 mm-width. The tissue properties [33] and corresponding thicknesses [34] are collected in Table 3. The lossy characterization of the human body tissues is commonly known. The most challenging tissue is the muscle because of its highest dielectric properties as can be seen from Table 3, at the 4 GHz center frequency. Even more, the muscle thickness differs from one person to another, but its value will be assumed 12 mm in these investigations. On the other hand, fat tissue is considered the most likely tissue changing its amount within people. In this context, a recent pioneer research [35] investigated the radio propagation at the 3.75–4.25 GHz UWB with a high directive antenna

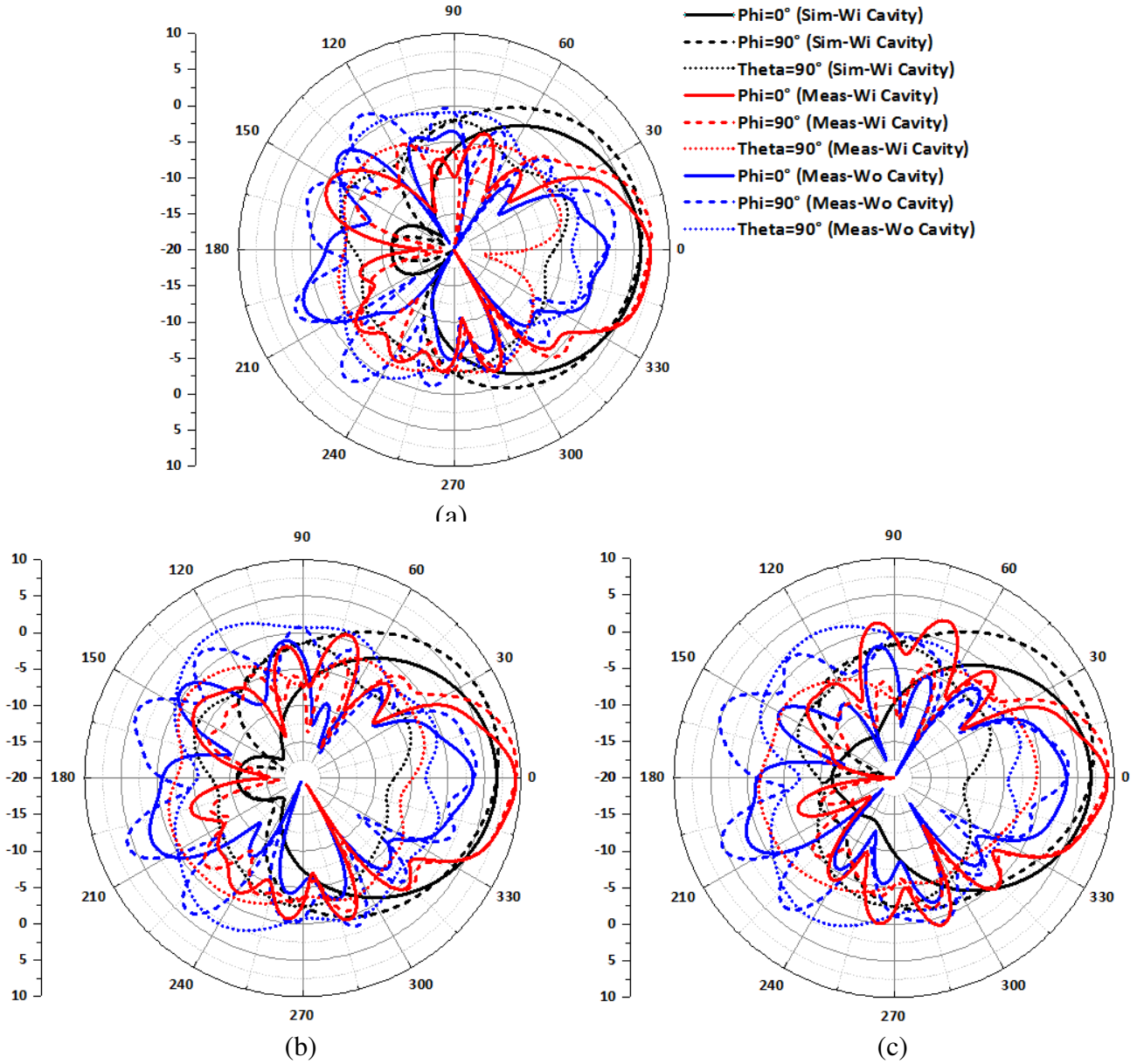

Figure 8. Simulated and measured radiation patterns in dB of the UWB antenna with "Wi" and without "Wo" cavity at (a) 3.75 GHz, (b) 4 GHz and (c) 4.25 GHz.

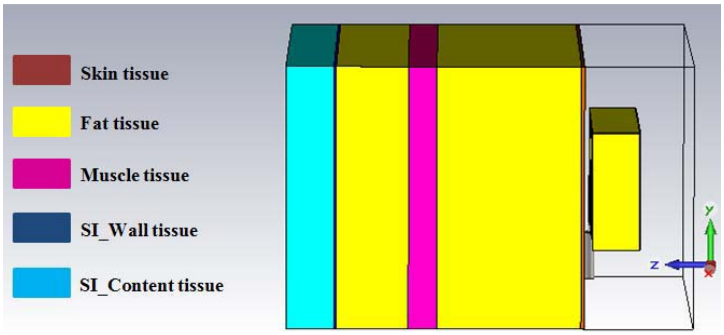

Figure 9. Abdominal multi-layer model used in simulations.

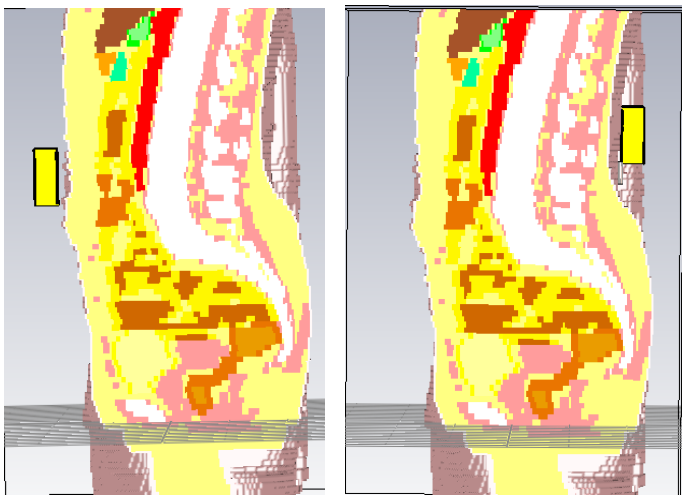

Figure 10. Antenna emplacement on the (a) navel and (b) back regions of the voxel model used in simulations.

Table 3. Tissue properties of the multi-layer model at 4 GHz [33].

Tissue layer	Density [kg/m^3]	Conductivity [S/m]	Permittivity	Thickness [mm]
Skin	1100	2.701	40.85	1.4
Fat1	910	0.1829	5.125	20/30/60
Muscle	1041	3.015	50.82	12
Fat2	910	0.1829	5.125	20/30/60
SI Wall	1020	3.015	50.82	1
SI Content	1020	4.622	51.63	20

through the fat layer. The focus was given to the several multi-path preferences of the propagated signal through the abdominal (Fat2) and visceral (Fat1) fat tissues on Laura voxel model. In this context, a set of fat-thickness combinations are chosen as grouped in Table 4 with the aim to evaluate the thickness impact on the antenna matching properties. The distance separating the antenna from the body model is selected to $d = 4$ mm. This 4 mm-distance is considered the minimal logical distance if the measurements will be conducted using a candidate wearing clothes. In fact, we assume that the average thickness of thin clothes is 4 mm. The multi-layer model basically emulates the abdominal area

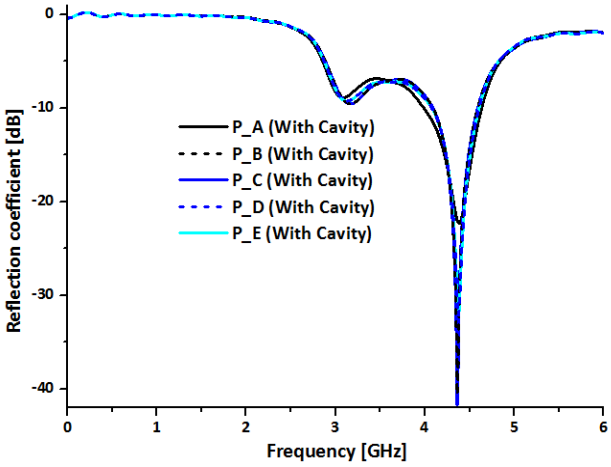

Figure 11. Simulated reflection coefficient of the UWB antenna with the cavity close to different multi-layer model cases.

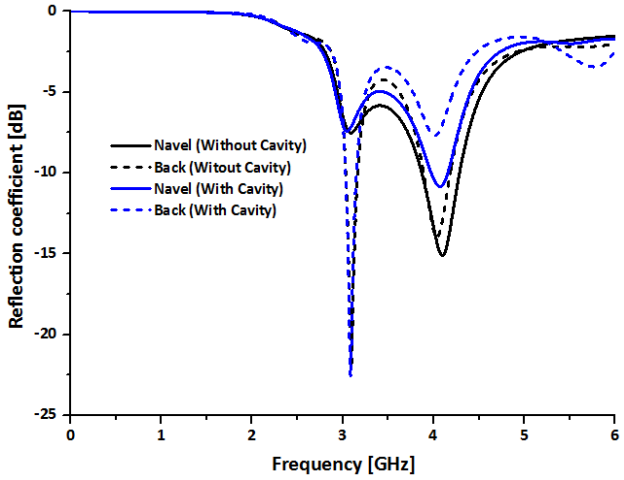

Figure 12. Simulated reflection coefficient of the UWB antenna with and without the cavity close to Navel and Back regions of the voxel model.

Table 4. Study case details of the multi-layer model.

Multi-layer model case	Fat1 [mm]	Fat2 [mm]
P_A	20	20
P_B	30	30
P_C	30	60
P_D	60	30
P_E	60	60

of the body. The multi-layer based results predict that the requested frequency band of 3.75–4.25 GHz is covered for reflection coefficient below −6 dB, as presented in Figure 11, and that the antenna matching is not sensitive to the fat amount. The matching characteristic is enabled/verified if the reflection coefficient is below −10 dB over the frequency band of interest. As the layered based model does not take into account the body curvature/shape and the complex organs, these studies were completed by voxel-based simulations. However, this time not only the abdomen area was under concern but the back area of the voxel model as well. In other terms, Figure 10(a) illustrates the antenna emplacement at 4 mm from the navel of the voxel model (considered the central point of the abdomen region), while Figure 10(b) illustrates the antenna position on the back region in an aligned line to the navel and at the same distance d. Simulated results conducted with the abdominal layered model show that the impedance bandwidth of the antenna with the cavity is expected to shift upwards to 4.0–4.6 GHz from free-space result, as can be seen from Figure 11. Then, this matching investigation on the abdominal body region was evaluated by situating the antenna on the navel of the voxel model, as plotted in Figure 12. The matching characteristic is ensured if the reflection coefficient is below −10 dB. This similar result corresponding to "Navel (With-Cavity)" shows that the antenna is mismatched. The mismatch issue can be seen from Figure 12 showing that the reflection coefficient does not even reach −10 dB at 3.75–4.25 GHz frequency band. Hence, the requested 3.75–4.25 GHz band is uncovered for this studied on-body case. Even more, this antenna mismatch is remarked as well at the back of the voxel model, as shown in Figure 12. Once the cavity is removed, the antenna starts to match to the navel and back of the voxel model, and the requested frequency band becomes covered. In other words, in this particular case, the reflection coefficient is below −10 dB over 3.75–4.25 GHz requested frequency band. The input impedance plots in Figure 13 show the capacitive impact of the proposed antenna

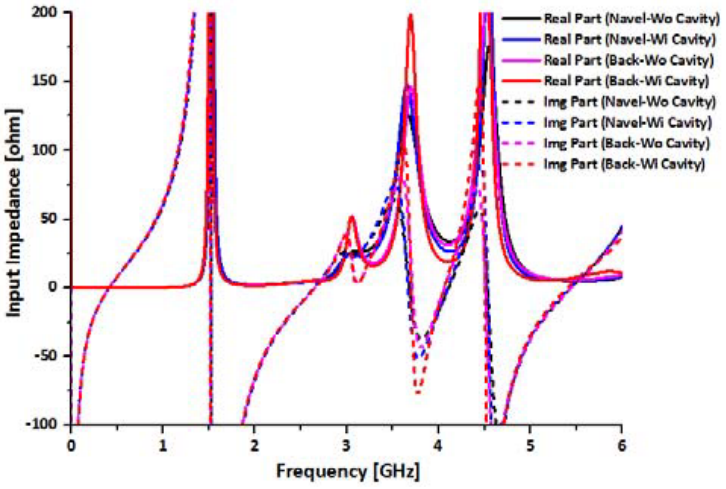

Figure 13. Simulated input impedance of the UWB antenna with and without the cavity close to Navel and Back regions of the voxel model.

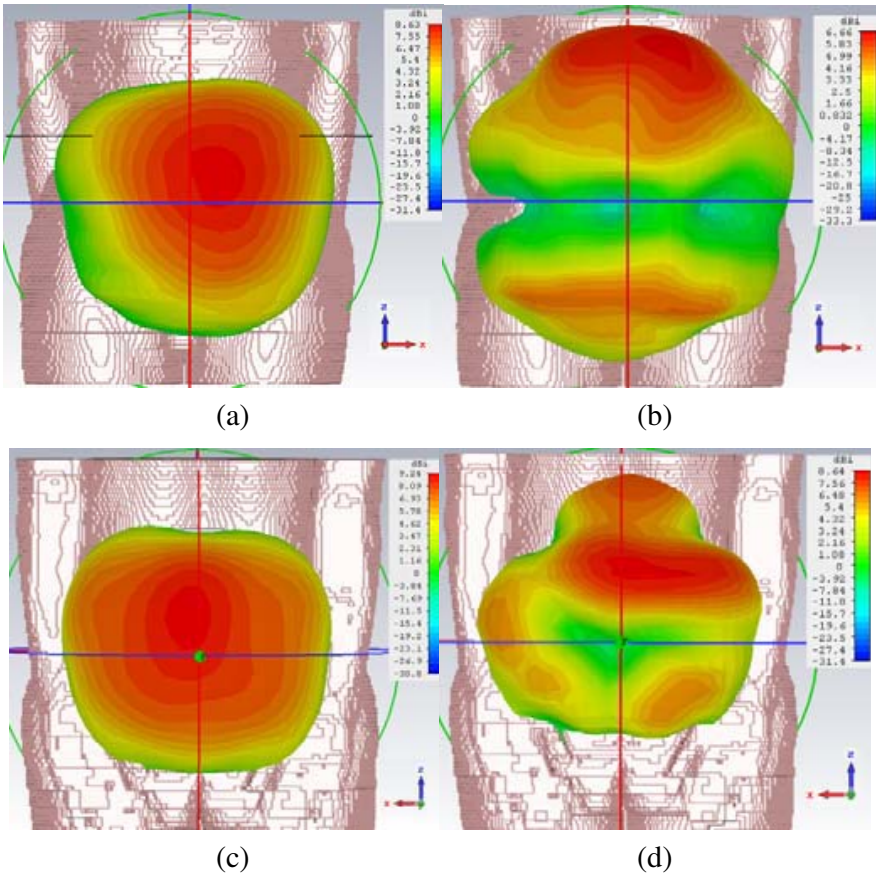

Figure 14. 3D directivity overview at 4 GHz of the UWB antenna using voxel model for the cases: (a) navel-Wo cavity, (b) navel-Wi cavity, (c) back-Wo cavity, (d) back-Wi cavity.

next to the voxel model. Besides, the antenna resistance is in 22–38 Ω range and is deteriorated from the 50 Ω free-space value. Moreover, this value failed with cavity presence regardless of the antenna emplacement (navel or back). The overview of the 3D directivity of the antenna with cavity close to the

Table 5. Radiation details of the UWB antenna with the cavity close to the different multi-layer models.

d = 4 mm	**Directivity [dBi]**	**Realized Gain [dB]**
Multi-layer (P_A)	8.7	−9.71
Multi-layer (P_B)	9.71	−7.65
Multi-layer (P_C)	9.75	−7.71
Multi-layer (P_D)	9.1	−8.52
Multi-layer (P_E)	9.03	−8.63

Table 6. Radiation details and the input impedance of the UWB antenna with and without the cavity close to the Navel and Back of the voxel model.

d = 4 mm	**Directivity [dBi]**	**Realized Gain [dB]**	**Input Impedance [Ω]**
Voxel_Navel (Without-Cavity)	8.6	2.1	$38.7 - j16.24$
Voxel_Navel (With Cavity)	6.7	−8.6	$30.9 - j17.3$
Voxel_Back (Without Cavity)	9.24	5.7	$34.8 - j11.2$
Voxel_Back (With Cavity)	8.64	−2.15	$21.9 - j13.2$

voxel model is given in Figure 14. On-body simulated directivity and maximum gain are presented in Figure 14, and results are collected in Table 5 and Table 6. From Table 5 based on multi-layer findings, the directivity and realized gain at 4 GHz seem to have average at 9 dBi and −8 dB, respectively. For a similar case on the navel of voxel model, the realized gain is quite the same while the directivity is less by 2 dB. Those values are more reliable since the voxel model is closer to the anatomy of a real human, including all the organs and averaging the tissue-thicknesses of a normal/thin human. Referring to Table 6, the directivity and realized gain tend to decrease with the cavity presence. Even more, the reported results on the back are improved compared with the navel-based results. The difference in the radiation properties of the antenna is due to the different natures and thicknesses of the human tissues inside the voxel model in the abdominal and back human parts.

When approaching on-body practical application, SAR (Specific Absorption Rate) estimations are indispensable [36, 37]. This parameter tells about the safety issue of the antenna pursuant to approved IEEE C95.3 standard [38]. According to [31], maximum reported SAR values are 0.78 mW/kg and 0.82 mW/kg for 10 g averaged mass with and without the cavity, respectively. These values are far less than the maximum allowed value of 2 W/kg. Besides, the power allowed (accepted) by the standard is 0.0029 W. The absorbed powers by our tissue volume under simulations are 0.0025 W and 0.0018 W for the antenna with and without the cavity, respectively, which are less than the accepted one reported by the standard. As a result, none of the antenna cases present any health risk on the human body.

5. SIMULATION ANALYSIS FOR INTRA-BODY COMMUNICATIONS

In this section, the intra-body propagation of the proposed UWB antenna within the different tissues of the human body is discussed. First, the investigations are conducted on the layered model, then results were compared to voxel model studies. At this regard, a set of E-field and H-field probes are located at the tissue interfaces of skin, fat1, muscle, fat2, SI_Wall, and SI_Content layers. The power is averaged by calculating the Poynting vector [39].

An overview of the disposition of the E/H-field probes on the abdominal part using the layered model and voxel models can be found in Figure 15 and Figure 16, respectively. Figure 16(b) provides an insight of the probes location inside the back of voxel model. The probes were displayed in such a way to average the power values from the skin surface to the end of the first SI segment, faced from the

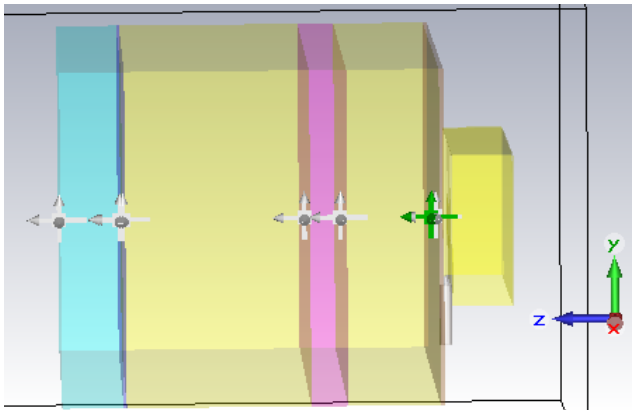

Figure 15. Power-probes locations for in-body propagation using multi-layer model.

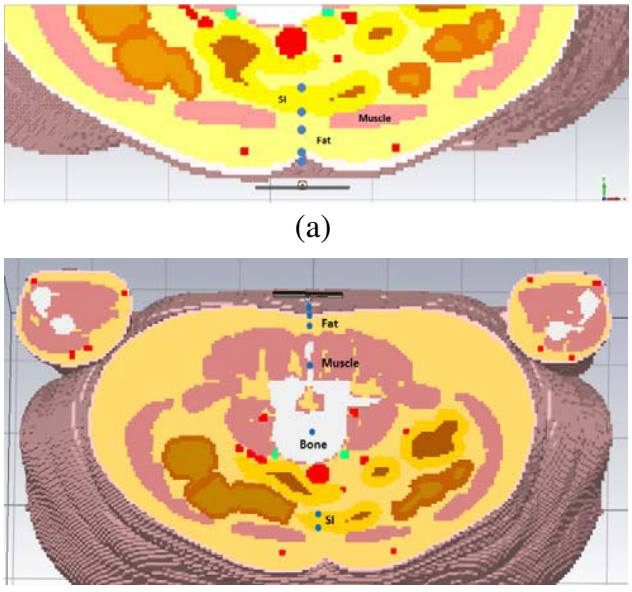

Figure 16. Power-probes locations for in-body propagation on the (a) navel and (b) back of the voxel model.

Table 7. Poynting vector — related results for intra-body propagation of the UWB antenna with cavity using the multi-layer model.

Power-field value [dB]	**P_A**	**P_B**	**P_C**	**P_D**	**P_E**
Skin	0	0	0	0	0
Fat1	−2.03	−2.55	−2.52	−2.47	−2.47
Muscle	−10.56	−14.76	−14.71	−23.57	−29.96
Fat2	−20.77	−24.62	−24.93	−33.18	−33.44
SI Wall	−28.44	−34.77	−41.85	−41.74	−48.07
SI Start	−29.26	−35.7	−42.58	−42.34	−48.73
SI End	−50.76	−56.81	−63.58	−63.37	−69.66
Averaged value [dB]	**50.76**	**56.81**	**63.58**	**63.37**	**69.66**

abdominal part, for the cases that the antenna is placed on the navel or the back side of the human body. Collected E-field and H-field complex values were saved and processed using Poynting Equation (1) described as follows:

$$S\,[\mathrm{dB}] = 10 * \log 10 \left(\left| \frac{1}{2} \mathrm{Real}(E \times H^*) \right| \right) \tag{1}$$

$\times$: Cross product. $*$: Conjugate value. E and H are the electric and magnetic complex vectors provided by the field probes, respectively.

Table 7 lists the calculated power, using Equation (1), reaching each tissue for the layered model cases. It is clearly seen from the table that 10 mm-thickness increase in both Fat layers produces/leads to 6 dB-value raise. Besides, by either increasing the thickness of Fat1 or Fat2 by 30 mm, the power is increased by 6 dB. However, when considering person case "P_E" with a large amount of fat about 60 mm, the estimated power loss is 70 dB. These aforementioned results were obtained using the proposed UWB antenna with cavity. These results are later compared using simulations on the abdominal part of

Table 8. Poynting vector — related results for intra-body propagation of the UWB antenna with and without cavity on the Navel and Back of voxel model.

	Navel_Area			Back_Area	
Probes	**Wo-cavity**	**Wi-cavity**	**Probes**	**Wo-cavity**	**Wi-cavity**
JBS	0	0	JBS	0	0
Skin	−2.5	−2.4	Skin	−4.6	−3.82
Fat	−1.4	−0.8	Fat	−6.6	−6.3
SI Start	−4.7	−4.7	Muscle	−30.7	−15.7
SI End	−22.2	−20.8	Bone	−52.7	−57.7
			SI Start	−87.8	−79.1
			SI End	−79.23	−69.3
Averaged value [dB]	**22.2**	**20.8**	**Averaged value [dB]**	**79.23**	**69.3**

voxel model, as illustrated in Figure 16(a). Table 8 shows that the averaged calculated power loss from the skin to the SI_end surfaces is 20.8 dB on the navel part using the cavity, while a smooth increase of 1.4 dB is remarked by taking off the cavity. However, this increase is insignificant and can be neglected in this study. Hence for practical use, the planar antenna without the cavity is largely enough to be used for wireless capsule endoscopy communication systems. Next, the antenna was assessed on the back area of the voxel model, and results can be found in Table 8. The simulated averaged power losses at the back with and without the cavity are 70 dB and 80 dB, respectively. This power loss increase demonstrates how the cavity strengthens the antenna directivity to penetrate deep tissues, and as a consequence, the consumed power is less. This navel/backed comparison was made only to show how significant is the impact of different tissues natures on the in-body propagation using 3.75–4.25 GHz UWB. For the medical application under concern in this paper, it is obvious that placing the antenna on the navel is an optimal and efficient solution to establish a good communication link with any capsule inside the SI tract. By comparing the voxel model result with layered-model, it is evident that the power is far less using the voxel. This is argued by the fact that the radio wave signals transmitted by the on-body antenna will choose a prior/easy way to propagate through the human body. According to a recent study [35], the signal is more likely assumed to propagate through fat layers.

6. ON-BODY ANTENNA MEASUREMENT ANALYSIS

To confirm the on-body application of the proposed UWB antenna, measurements were conducted on a real human subject. Therefore, a set of measurement scenarios were under test related to the on-body emplacement of the prototype on the real human as described in Figure 17. The on-body measurement setups using the proposed UWB antenna with and without the cavity are found in Figures 18(a) and (b), respectively. The antenna was kept directly on the body clothes of the human subject for ($d = 0$ mm). Initially, the proposed UWB antenna was measured without cavity, as shown in Figure 18(a), at different on-body emplacements described in Figure 17. Measured reflection coefficient shows, according to Figure 19, that the direct contact of the antenna through thin clothes widened the bandwidth to 3.36–5.12 GHz compared to free-space measured results. This on-body matching result is favorable because it concludes that the requested bandwidth of 3.75–4.25 GHz is still covered/maintained. Hence, measured matching results are in good agreement with the simulated ones presented in Figure 12. Meanwhile, according to Figure 20, the antenna is mismatched with the distance increase from 2 mm to 10 mm. However, over ($d = 10$ mm) the antenna starts to match close to the body and are more close to free-space results. This is predictable as the antenna changes the behavior next to human body with the distance change according to the reactive near-field of the antenna as analyzed in [40]. In the case that the cavity is backing the proposed antenna, the antenna is mismatched at $d = 0$ mm regardless of the on-body emplacement, as can be seen from Figure 21. According to Figure 22, this impedance mismatch

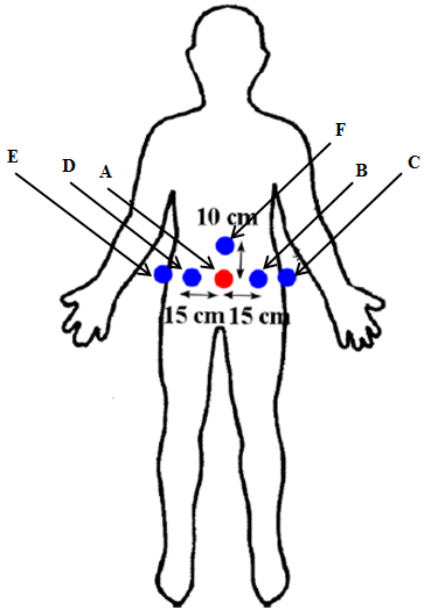

Figure 17. On-body measurement scenarios.

(a) (b)

Figure 18. On-body measurement setup using the proposed UWB antenna (a) without and (b) with cavity.

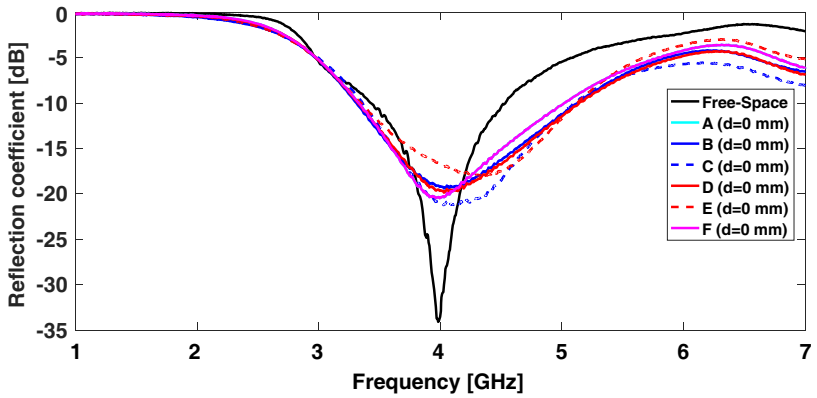

Figure 19. Measured reflection coefficient of the proposed UWB antenna without cavity at different on-body parts with ($d = 0\,\text{mm}$).

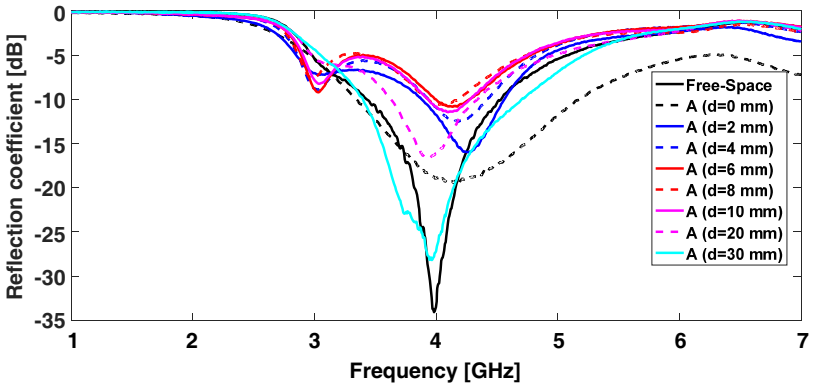

Figure 20. Measured reflection coefficient of the proposed UWB antenna without cavity at the navel position with different distances d.

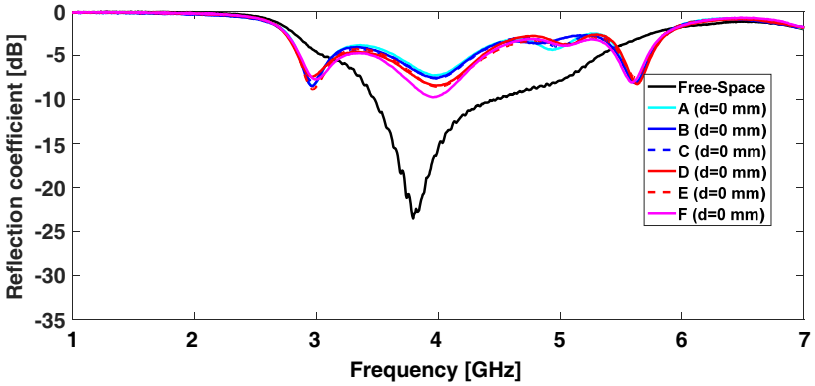

Figure 21. Measured reflection coefficient of the proposed UWB antenna with cavity at different on-body parts with ($d = 0$ mm).

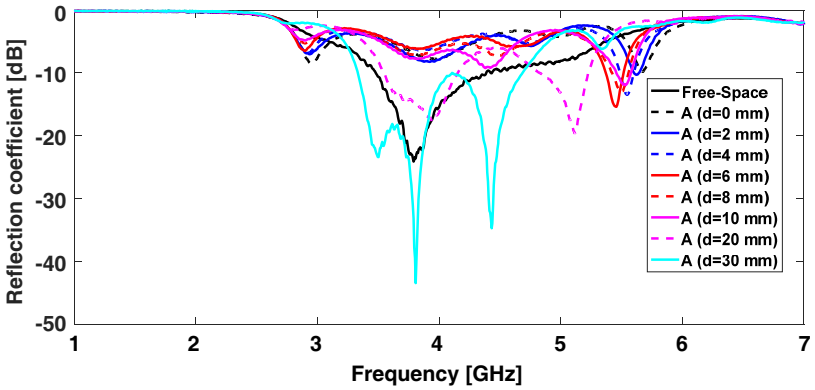

Figure 22. Measured reflection coefficient of the proposed UWB antenna with cavity at the navel position with different distances d.

remains up to $d = 10$ mm. However, beyond this distance the requested bandwidth of 3.75–4.25 GHz is covered, as plotted in Figure 22. Accurately, the measured bandwidths are 3.52–4.25 GHz and 3.32–4.72 GHz at $d = 20$ mm and $d = 30$ mm for the antenna with cavity, respectively. These measurements findings are in good agreement with on-body voxel simulations presented previously in Section 4, and validate the privilege of choosing the proposed antenna without cavity in real medical use.

7. CONCLUSION AND PERSPECTIVES

The UWB antenna introduced in this paper is targeted for on-body BAN (Body Area Networks) application. The antenna is tested with and without the cavity in free-space and on-body environments. Initially, simulation studies were conducted to accurately design the antenna. Free-space measurements demonstrate good performance of the proposed antenna with 5.78 dB and 9.50 dB gain values towards the body direction, without and with the cavity, respectively. In this context, the proposed antenna can be used in couple of applications, i.e., heart beat and respiratory rate monitoring using low-UWB frequency, etc. Later, voxel model-based simulations were conducted to converge to realistic on-body environment in addition to multi-layer model. These voxel investigations were not bounded on the abdominal area, and the back area of the voxel model was examined as well. The on-body testing englobes the bandwidth matching of the antenna with and without cavity, as well as the power consumption of different body environments. As predicted, the averaged power loss consumed by the back tissues further exceeds the abdominal tissues by 49 dB and 58 dB with and without the cavity, respectively. Hence, planar antenna (without cavity) was regarded as a good antenna option for this particular medical application on the abdominal human part. Next, the on-body antenna operation was confirmed by a real human holding the antenna with and without the cavity, and different body locations and body distances were taken into account. On-body measured results endorse the good resulting matching in the case of the planar antenna alone. As a result, the antenna without cavity on abdominal area was selected and privileged for wireless capsule endoscopy application. In the following investigations, the channel propagation will be evaluated using different voxel models and confirmed by on-body measurements on different thin and overweight persons. Another paper will be devoted to assess the communication link between the proposed antenna and a capsule by simulations and measurements.

ACKNOWLEDGMENT

This research was funded by the Academy of Finland 6 Genesis Flagship, grant number 318927.

REFERENCES

1. Bharadwaj, R., S. Swaisaenyakorn, C. G. Parini, J. C. Batchelor, and A. Alomainy, "Impulse radio ultra-wideband communications for localization and tracking of human body and limbs movement for healthcare applications," *IEEE Trans. Antennas Propag.*, Vol. 65, No. 12, 7298–7309, 2017.
2. Strackx, M., E. D'Agostino, P. Leroux, and P. Reynaert, "Direct RF subsampling receivers enabling impulse-based UWB signals for breast cancer detection," *IEEE Trans. Circuits Syst. II Express Briefs*, Vol. 62, No. 2, 144–148, 2015.
3. Wang, S., Y. Ji, D. Gibbins, and X. Yin, "Impact of dynamic wideband MIMO body channel characteristics on healthcare rehabilitation of walking," *IEEE Antennas Wirel. Propag. Lett.*, Vol. 16, 505–508, 2017.
4. Li, Y. and M. Zhang, "Study on a cylindrical sensor network for intelligent health monitoring and prognosis," *IEEE Access*, Vol. 6, 69195–69202, 2018.
5. Li, Y., L. Yang, W. Duan, and X. Zhao, "An implantable antenna design for an intelligent health monitoring system considering the relative permittivity and conductivity of the human body," *IEEE Access*, Vol. 7, 38236–38244, 2019.
6. Vispa, A., L. Sani, M. Paoli, A. Bigotti, G. Raspa, N. Ghavami, S. Caschera, M. Ghavami, M. Duranti, and G. Tiberi, "UWB device for breast microwave imaging: Phantom and clinical validations," *Measurement*, Vol. 146, 582–589, 2019.
7. Niendorf, T., T. Huelnhagen, L. Winter, and K. Paul, "13 — Human cardiac magnetic resonance at ultrahigh fields: Technical innovations, early clinical applications and opportunities for discoveries," *Cardiovascular Magnetic Resonance (Third Edition)*, 142–160.e4, 2019.
8. Chen, C.-A., S.-L. Chen, C.-H. Lioa, and P. A. R. Abu, "Lossless CFA image compression chip design for wireless capsule endoscopy," *IEEE Access*, Vol. 7, 107047–107057, 2019.

9. Charfi, S., M. E. Ansari, and I. Balasingham, "Computer-aided diagnosis system for ulcer detection in wireless capsule endoscopy images," *IET Image Process.*, Vol. 13, No. 6, 1023–1030, 2019.
10. Hoang, M. C., V. H. Le, J. Kim, E. Choi, B. Kang, J.-O. Park, and C.-S. Kim, "Untethered robotic motion and rotating blade mechanism for actively locomotive biopsy capsule endoscope," *IEEE Access*, Vol. 7, 93364–93374, 2019.
11. Munoz, F., G. Alici, H. Zhou, W. Li, and M. Sitti, "Analysis of magnetic interaction in remotely controlled magnetic devices and its application to a capsule robot for drug delivery," *IEEE ASME Trans. Mechatron.*, Vol. 23, No. 1, 298–310, 2018.
12. Leung, B. H. K., C. C. Y. Poon, R. Zhang, Y. Zheng, C. K. W. Chan, P. W. Y. Chiu, J. Y. W. Lau, and J. J. Y. Sung, "A therapeutic wireless capsule for treatment of gastrointestinal haemorrhage by balloon tamponade effect," *IEEE Trans. Biomed. Eng.*, Vol. 64, No. 5, 1106–1114, 2017.
13. Charthad, J., M. J. Weber, T. C. Chang, and A. Arbabian, "A mm-sized implantable medical device (IMD) with ultrasonic power transfer and a hybrid bi-directional data link," *IEEE J. Solid-State Circuits*, Vol. 50, No. 8, 1741–1753, 2015.
14. Barbi, M., C. G.-Pardo, A. Nevárez, V. P. Beltrán, and N. Cardona, "UWB RSS-based localization for capsule endoscopy using a multilayer phantom and in vivo measurements," *IEEE Trans. Antennas Propag.*, Vol. 67, No. 8, 5035–5043, 2019.
15. Shao, G., Y. Tang, L. Tang, Q. Dai, and Y.-X. Guo, "A novel passive magnetic localization wearable system for wireless capsule endoscopy," *IEEE Sens. J.*, Vol. 19, No. 9, 3462–3472, 2019.
16. Alam, M. W., Md. M. Hasan, S. K. Mohammed, F. Deeba, and K. A. Wahid, "Are current advances of compression algorithms for capsule endoscopy enough? A technical review," *IEEE Rev. Biomed. Eng.*, Vol. 10, 26–43, 2017.
17. Miah, Md. S., A. N. Khan, C. Icheln, K. Haneda, and K.-I. Takizawa, "Antenna system design for improved wireless capsule endoscope links at 433 MHz," *IEEE Trans. Antennas Propag.*, Vol. 67, No. 4, 2687–2699, 2019.
18. Peng, Y., K. Saito, and K. Ito, "Dual-band antenna design for wireless capsule endoscopic image transmission in the MHz band based on impulse radio technology," *IEEE J. Electromagn. RF Microw. Med. Biol.*, Vol. 3, No. 3, 158–164, 2019.
19. Duan, Z., L.-J. Xu, S. Gao, and W. Geyi, "Integrated design of wideband omnidirectional antenna and electronic components for wireless capsule endoscopy systems," *IEEE Access*, Vol. 6, 29626–29636, 2018.
20. Chu, H., P.-J. Wang, X.-H. Zhu, and H. Hong, "Antenna-in-package design and robust test for the link between wireless ingestible capsule and smart phone," *IEEE Access*, Vol. 7, 35231–35241, 2019.
21. Lei, W. and Y.-X. Guo, "Design of a dual-polarized wideband conformal loop antenna for capsule endoscopy systems," *IEEE Trans. Antennas Propag.*, Vol. 66, No. 11, 5706–5715, 2018.
22. IEEE Standard for Local and metropolitan area networks — Part 15.6: Wireless Body Area Networks, IEEE Std 802.15.6-2012.
23. ISO/IEC/IEEE International Standard — Information technology — Telecommunications and information exchange between systems — Local and metropolitan area networks — Specific requirements — Part 15-6: Wireless body area network, ISO/IEC/IEEE 8802-15-6:2017(E).
24. Thotahewa, K. M. S., J.-M. Redoutè, and M. R. Yuce, "Propagation, power absorption, and temperature analysis of UWB wireless capsule endoscopy devices operating in the human body," *IEEE Trans. Microw. Theory Tech.*, Vol. 63, No. 11, 3823–3833, 2015.
25. Dissanayake, T., M. R. Yuce, and C. Ho, "Design and evaluation of a compact antenna for implant-to-air UWB communication," *IEEE Antennas Wirel. Propag. Lett.*, Vol. 8, 153–156, 2009.
26. Anzai, D., K. Katsu, R. C. Santiago, Q. Wang, D. Plettemeier, J. Wang, and I. Balasingham, "Experimental evaluation of implant UWB-IR transmission with living animal for body area networks," *IEEE Trans. Microw. Theory Tech.*, Vol. 62, No. 1, 183–192, 2014.

27. Wang, Q., K. Wolf, and D. Plettemeier, "An UWB capsule endoscope antenna design for biomedical communications," *2010 3rd International Symposium on Applied Sciences in Biomedical and Communication Technologies (ISABEL 2010)*, Rome, Italy, 2010.
28. Ahmed, G., S. U. Islam, M. Shahid, A. Akhunzada, S. Jabbar, M. K. Khan, M. Riaz, and K. Han, "Rigorous analysis and evaluation of specific absorption rate (SAR) for mobile multimedia healthcare," *IEEE Access*, Vol. 6, 29602–29610, 2018.
29. Bisheh, K. M., M. G. Miab, and B. Zakeri, "Evaluation of different approximations for correlation coefficients in stochastic FDTD to estimate SAR variance in a human head model," *IEEE Trans. Electromagn. Compat.*, Vol. 59, No. 2, 509–517, 2017.
30. Simbor, S. P., C. Andreu, C. G. Pardo, M. Frasson, and N. Cardona, "UWB path loss models for ingestible devices," *IEEE Trans. Antennas Propag.*, Vol. 67, No. 8, 5025–5034, 2019.
31. Kissi, C., M. Särestöniemi, T. Kumpuniemi, M. Sonkki, S. Myllymäki, M. N. Srifi, and C. P. Raez, "Low-UWB receiving antenna for WCE localization," *13th International Symposium on Medical Information and Communication Technology (ISMICT)*, Oslo, Norway, 2019.
32. https://www.rohacell.com/product/peekindustrial/downloads/rohacell%20hf%20product%20information.pdf.
33. https://www.itis.ethz.ch/virtual-population/tissue-properties/database/dielectric-properties/.
34. Akkus, O., A. Oguz, M. Uzunlulu, and K. Kizilgul, "Evaluation of skin and subcutaneous adipose tissue thickness for optimal insulin injection," *J. Diabetes Metab.*, Vol. 3, No. 8, 1–5, 2012.
35. Särestöniemi, M., C. P. Raez, C. Kissi, T. Kumpuniemi, M. Sonkki, M. Hämäläinen, and J. Iinatti, "Fat in the Abdomen area as a propagation medium in WBAN applications," *Body Area Networks: Smart IoT and Big Data for Intelligent Health Management*, *14th EAI International Conference, BODYNETS 2019*, 175–187, Florence, Italy, 2019.
36. C95.7-2014 — IEEE Recommended Practice for Radio Frequency Safety Programs, 3 kHz to 300 GHz, IEEE Std C95.7-2014 (Revision of IEEE Std C95.7-2005).
37. C95.2-2018 — IEEE Standard for Radio-Frequency Energy and Current-Flow Symbols, IEEE Std C95.2-2018 (Revision of IEEE Std C95.2-1999).
38. C95.3-2002 — IEEE Recommended Practice for Measurements and Computations of Radio Frequency Electromagnetic Fields With Respect to Human Exposure to Such Fields, 100 kHz–300 GHz, IEEE Std C95.3-2002 (Revision of IEEE Std C95.3-1991), 1–126, 2003.
39. Balanis, C. A., *Antenna Theory Analysis and Design*, 3rd edition, 27–68, John Wiley & Sons Ltd, 2005.
40. Tuovinen, T., M. Berg, K. Y. Yazdandoost, and J. Iinatti, "Ultra wideband loop antenna on contact with human body tissues," *IET Microwaves, Antennas & Propagation*, Vol. 7, No. 7, 588–596, 2013.